This manuscript was originally submitted to the *Bulletin of the Seismological Society of America* on December 28, 2024. It has undergone peer review and is currently under revision.

Bulletin of the Seismological Society of America

Predictable and Unpredictable Aspects of Earthquakes from P-wave Onsets: Vigorous Ruptures Finish Quickly

--Manuscript Draft--

Manuscript Number:	BSSA-D-24-00282
Article Type:	Article
Section/Category:	Regular Issue
Full Title:	Predictable and Unpredictable Aspects of Earthquakes from P-wave Onsets: Vigorous Ruptures Finish Quickly
Corresponding Author:	Satoshi Ide University of Tokyo Tokyo, JAPAN
Corresponding Author's Institution:	University of Tokyo
Corresponding Author E-Mail:	ide@eps.s.u-tokyo.ac.jp
Order of Authors:	Satoshi Ide
	Keisuke Yoshida
Abstract:	ABSTRACT It is widely acknowledged that predicting the final size of an earthquake from the P-wave onset in seismograms is nearly impossible. However, this study explores whether there are any predictable aspects of the rupture process from the initial P-wave. We propose that the moment-normalized duration of an earthquake negatively correlates with its initial stress drop, which is measured from the slope (parameter [[EQUATION]]) of the acceleration record shortly after onset. Since 2007, [[EQUATION]] has been used in the Japanese earthquake early warning system as an indicator of epicentral distance, yet it also provides deeper insights into earthquake dynamics and wave propagation. Utilizing high-sensitivity seismograms from approximately 800 borehole stations in Hi-net and combining manually picked P-wave arrival times and focal mechanisms for about 1800 earthquakes, we estimate [[EQUATION]] for each station and earthquake pair within a 0.1 s window. We confirm that [[EQUATION]] decreases from the square to the fourth power of the P-wave travel time, a phenomenon not explainable by simple geometric decay or intrinsic attenuation alone. Residuals between observed values and travel time dependencies are further decomposed into event and site terms, alongside radiation pattern dependency, which is close to a power of 0.5—possibly reflecting complex rupture processes that begin at a minute scale. The event term primarily represents the initial stress drop, showing minimal dependency on final size and a clear dependency on event depth, mirroring observations of average stress drop. This term also shows a statistically significant correlation with the moment-normalized duration estimated independently using S-waves, suggesting limited predictability of the rupture process. The site terms, which correlate with tectonic structure, help reduce errors in estimating arrival times, especially for nearby earthquakes, thus offering practical benefits for early warning systems.
Author Comments:	
Suggested Reviewers:	

Opposed Reviewers:	
Additional Information:	
Question	**Response**
Key Point #1: <i>Three key points will be printed at the front of your manuscript so readers can get a quick overview. Please provide three COMPLETE sentences addressing the following: 1) state the problem you are addressing in a FULL sentence; 2) state your main conclusion(s) in a FULL sentence; and 3) state the broader implications of your findings in a FULL sentence. Each point must be 110 characters or less (including spaces).	P-wave acceleration onset is size-independent but informs on the path, source, and site characteristics.
Key Point #2:	Large initial stress drops lead to quicker ruptures for earthquakes of a given size.
Key Point #3:	Site terms correlate with tectonic structures and can be utilized for earthquake early warning.

Predictable and Unpredictable Aspects of Earthquakes from P-wave Onsets: Vigorous Ruptures Finish Quickly

Satoshi Ide[1] and Keisuke Yoshida[2]

1. Department of Earth and Planetary Science, Graduate School of Science, The University of Tokyo, Tokyo, Japan

2. Research Center for Prediction of Earthquakes and Volcanic Eruptions, Graduate School of Science, Tohoku University, Sendai, Japan

Corresponding author: ide@eps.s.u-tokyo.ac.jp

KEY POINTS (110 characters including space)

- P-wave acceleration onset is size-independent but informs on the path, source, and site characteristics.
- Large initial stress drops lead to quicker ruptures for earthquakes of a given size.
- Site terms correlate with tectonic structures and can be utilized for earthquake early warning.

ABSTRACT (300 words)

It is widely acknowledged that predicting the final size of an earthquake from the P-wave onset in seismograms is nearly impossible. However, this study explores whether there are any predictable aspects of the rupture process from the initial P-wave. We propose that the moment-normalized duration of an earthquake negatively correlates with its initial stress drop, which is measured from the slope (parameter B) of the acceleration record shortly after onset. Since 2007, B has been used in the Japanese earthquake early warning system as an indicator of epicentral distance, yet it also provides deeper insights into earthquake dynamics and wave propagation. Utilizing high-sensitivity seismograms from approximately 800 borehole stations in Hi-net and combining manually picked P-wave arrival times and focal mechanisms for about 1800 earthquakes, we estimate B for each station and earthquake pair within a 0.1 s window. We confirm that B decreases from the square to the fourth power of the P-wave travel time, a phenomenon not explainable by simple geometric decay or intrinsic attenuation alone. Residuals between observed values and travel time dependencies are further decomposed into event and site terms, alongside radiation pattern dependency, which is close to a power of 0.5—possibly reflecting complex rupture processes that begin at a minute scale. The event term primarily represents the initial stress drop, showing minimal dependency on final size and a clear

dependency on event depth, mirroring observations of average stress drop. This term also shows a statistically significant correlation with the moment-normalized duration estimated independently using S-waves, suggesting limited predictability of the rupture process. The site terms, which correlate with tectonic structure, help reduce errors in estimating arrival times, especially for nearby earthquakes, thus offering practical benefits for early warning systems.

(6000 words, 10 figures, 3 tables)

INTRODUCTION

The question of whether large and small earthquakes initiate differently has been debated for nearly three decades and is now nearing a resolution. Since the 1990s, insights from the physics of friction have highlighted the importance of the nucleation process at the initiation of earthquake rupture (Dieterich, 1992; Shibazaki and Matsu'ura, 1992). Around the same time, observations of earthquake waveforms indicated the presence of a slow initial phase, distinct from the subsequent seismic waves (Umeda, 1990; Ellsworth and Beroza, 1995; Iio, 1995). This led to debates on whether this initial phase is related to the nucleation process, and whether its characteristics depend on the final size of the earthquake (Ellsworth and Beroza, 1995; Iio, 1995; Mori and Kanamori, 1996). If the initial phase influences the final size of an earthquake, detecting its deterministic features could improve earthquake early warning (EEW) systems.

Since the 2000s, various methods have been proposed to predict the final size of earthquakes from the initial characteristics of seismic waves (Olson and Allen, 2005; Wu and Zhao, 2006; Festa et al., 2008; Colombelli et al., 2014). For example, Olson and Allen (2005) suggested that the initial phase has deterministic properties, and that the final size of an earthquake could be predicted based on the characteristics of the first four seconds of the seismic waves. However, this claim was refuted by Rydelek and Horiuchi (2006). In recent years, statistically robust analyses using large datasets have increasingly reported that the initial characteristics of seismic waves do not depend on the final size (Meier et al., 2016; Noda and Ellsworth, 2016; Trugman et al., 2019). There have been many cases where, despite producing very similar initial signals at many seismic stations, the final magnitudes differed by more than M1 (Ide, 2019). While it is premature to conclude that all earthquake rupture processes start in a statistically in undistinguishable way, it is certain that even if there are differences, detecting them is extremely difficult. Applications to EEW systems are not straightforward.

Nevertheless, it is possible to make some probabilistic forecast about the final size of an earthquake based on its initial seismic waves of finite duration. Using the finite time signal from the arrival of the P-wave, it is easy to distinguish between earthquakes that end within that duration and those that do not. Additionally, if the amplitude of seismic waves is increasing or decreasing at a certain moment, the likelihood of the earthquake growing larger is higher for the former. Since the observed seismic waves reflect the earthquake rupture process, quantitative forecast requires a mathematical description of the average rupture growth and its fluctuations. The simplest model that includes the necessary elements to describe initial seismic waves and rupture growth would be the infinite self-similar growth model of a circular crack (Kostrov, 1964), or the Sato & Hirasawa model (Sato and Hirasawa, 1973), which also includes a whole source-time function until the termination. In these models, the moment rate function and the observed displacement show a proportional increase with the square of time, which is consistent with observational data and serves as a useful low-level approximation (e.g., Uchide and Ide, 2010), until the approximation fails when the finiteness of the seismogenic layer becomes significant.

Observed seismic waves exhibit significantly more complexity than the predictions of such models. The complexity of seismic waves increases during wave propagation to the seismic station, but the complexity of the rupture process also contributes significantly. The source faults are far from planar, exhibiting fractal-like roughness on surfaces (Brown and Scholz, 1985; Power and Tullis, 1991; Candela et al., 2012), and rupture propagates in jerky motion over non-planar structures such as branches and steps. While rupture propagates from a point at a constant speed in average, closer examination reveals large deviations from the average, characterized by jerky progression. Understanding such deviations is crucial for interpreting both initial and overall seismic wave behaviors. Ide and Aochi (2005) described a model where fractally distributed circular patches rupture in a cascading-up manner, capturing the behavior of initial ruptures. This model accounts for observations of Olson and Allen (2005) (Yamada and Ide, 2008), the statistical properties of source time functions in large earthquakes (Renou et al., 2022), and the initiation of identical earthquakes (Ide, 2019). Although the model in Ide and Aochi (2005) was a planar model, real earthquake rupture occurs within a complex fault network in a three-dimensional medium (Gabriel et al., 2024). Determining which mathematical model is more appropriate can be constrained by comparing the predictability based on initial seismic wave observations.

The initial seismic waves can serve alternative purposes. One example is the method of estimating the distance to the source from the initial seismic waves. About 20 years ago, Odaka et al. (2003) and Tsukada et al. (2004) proposed a technique for estimating the epicentral distance from the first few seconds of P-wave record at a single station. They demonstrated that the amplitude of the "envelope" of the P-wave acceleration record can be approximated by

$$Bt\exp(-At) \tag{1}$$

where A and B are constants and t is time from the arrival. They showed that while the coefficient

B decreases with increasing epicentral distance Δ, it is nearly independent of earthquake magnitude. They developed a method to estimate Δ from B, naming it the $B - \Delta$ method. By calculating the epicentral distance using this method and simultaneously estimating the wave propagation direction using techniques such as principal component analysis of P-wave particle motion, the epicentral location can be determined from only the P-wave onset at the station where the seismic waves first arrive. As a type of EEW that estimates the source location from seismic waves, this is currently the fastest method for determining the source location. This scheme was incorporated into the EEW system of the Japan Meteorological Agency (JMA), which has been in practical use since 2007 (Hoshiba et al., 2008). It should be noted that at the limit as $t \to 0$, the above formula simplifies to Bt. Japan Railways has formalized this form as the $C - \Delta$ method for use in their EEW (Iwata et al., 2015), and while the calculations in this paper are similar to the $C - \Delta$ method, out of respect for the original, we refer to the $B - \Delta$ method.

The coefficient B decreases with Δ following a power law of approximately 2–4. This behavior defies straightforward explanation within conventional seismological frameworks. Geometric attenuation would result in a decrease proportional to the inverse of distance, while intrinsic attenuation would follow an exponential decay. Tsukada et al. (2004) attributed this phenomenon to forward scattering of P-waves and verified its plausibility through simple numerical simulations. However, subsequent investigations into this issue have been limited (e.g., Okamoto and Tsuno, 2019). If scattering plays a role, it is likely related to the heterogeneity of the subsurface structure. Additionally, B encapsulates information about the initial stress conditions at the source and the radiation pattern at high frequencies. Hence, the intriguing nature of parameter B calls for further in-depth investigation.

Therefore, this study reevaluates the $B - \Delta$ method in the context of current earthquake physics and assesses its relevance and importance. Specifically, we analyze moderate to large ($M > 3$) earthquakes in Japan with focal mechanism information, estimate values for B from high-quality borehole seismograms and manually picked P-wave arrivals. Subsequently, a functional relationship between source distance and B values is established and the unexplained factors are decomposed into contributions at the source, the site, and radiation pattern. We observe deviations from linearity in the dependency on radiation patterns. Moreover, the contribution at the source (source term) depends largely on the initial stress drop but shows little dependence on the final size. The source term also depends on depth, similar to the depth dependence of earthquake average stress drop. Most of the earthquakes studied here have had their source-time functions estimated by Yoshida and Kanamori (2023). Comparing the source term with the final duration reveals that shorter durations are observed when the source term is large. This suggests a negative correlation between initial stress drop and normalized duration and demonstrates the limited predictability of P-wave onset for the final characteristics of earthquakes.

DATA AND METHOD

Earthquakes, Seismograms, and Pick Information

In this study, we analyze earthquakes that occurred in Japan from 2004 to 2020. JMA detected these earthquakes, and the National Research Institute for Earth Science and Disaster Resilience (NIED) determined their moment tensor solutions. We reference the size of the earthquakes from these solutions using calculated seismic moments M_0 and moment magnitude M_W. We only consider earthquakes with source depths of 1-30 km and surrounded by observation stations. Specifically, we calculate azimuthal gaps between stations from the source, excluding any events with a maximum gap exceeding 180 degrees. We also exclude earthquakes located more than 50 km from the nearest station. Consequently, the dataset primarily consists of events occurring beneath the land area of Japan, totaling approximately 1800 events, as shown in Figure 1. Although we do not intentionally exclude earthquakes in subduction zones, we generally consider these to be inland earthquakes. The M_W values range from 3.1 to 7.1, but with the 5th and 95th percentiles at 3.3 and 4.7, respectively, this range mainly constitutes our primary data set.

We use data recorded by borehole high-sensitivity short-period seismometers at ~800 NIED Hi-net stations, as shown in Figure 1. The original data are proportional to ground velocity at higher frequencies than the pendulum frequency of 1 Hz, with a sampling rate of 100 samples per second. We use the vertical component of stations where JMA has provided pick information for the P-wave arrival. From the origin time and the P-wave arrival time at each station, we calculate the travel time T_p from the source to the station. We exclude stations with T_p greater than 25 s from the analysis. Assuming the velocity structure used in JMA's routine analysis (Ueno, 2002), we calculate the take-off angle of the P-wave at the source, and the radiation pattern R_p based on the moment tensor solutions. We exclude the data if $R_p < 0.1$.

Estimation and Interpretation of B Parameter

We quantify the onset of P-wave, following the $B - \Delta$ method. The manually picked arrival time is designated as t_0, and the seismic wave velocity at that time is v_0. The acceleration is calculated as $a_i = (v_i - v_{i-1})/dt$. For N acceleration samples, we estimate B that minimizes the sum of the squares of e_i in the following equation (Figures 2 and S1):

$$|a_i| = Bt_i + e_i, \qquad i = 0, \ldots, N-1. \tag{2}$$

In the original $B - \Delta$ method (Odaka et al., 2003), the left side of the equation is:

$$\max_{j\leq i}|a_i|. \tag{3}$$

As expected, the B values in the original definition are larger, but the difference has an average of 0.067 and a standard deviation of 0.079 in case $N = 10$ (Figure S2). This difference is not significant compared to the error in the subsequent analysis. Since we confirmed that there is no substantial difference in the results, we use the definition in equation (2) in this paper.

We tested sample sizes N of 10 - 40, with $dt = 0.01\ s$, corresponding to time window lengths of 0.1 to 0.4 seconds. This discussion focuses on the case of a time window of 0.01 and $N = 10$, with other sample sizes presented as necessary. We consider the period up to one second before t_0 as the noise period and perform quality control of the signal. We exclude waveforms where the standard deviation of acceleration samples during this period, σ_{noise}, exceeds $10^{-5}\ \mathrm{m/s^2}$. Similarly, waveforms where the standard deviation of the samples used to estimate B, σ_{signal}, is less than $\sqrt{10}\sigma_{noise}$ are also excluded from the analysis.

The formula (1) is empirically assumed. However, from the perspective of earthquake source processes and wave propagation theory, how can we hypothesize the initial shape of acceleration signals? The simplest source model that does not depend on the final size would be a self-similar circular crack extension with a constant stress drop (Kostrov, 1964; Sato and Hirasawa, 1973). In this case, the acceleration of the P-wave depends on a step function with the amplitude:

$$\frac{24}{7\pi}\Delta\sigma\frac{R^p}{\rho r}\frac{v^3}{\alpha^3}, \tag{4}$$

Where α and ρ are the P-wave speed and density of the medium, v is the rupture propagation velocity, $\Delta\sigma$ is the stress drop, r is the source distance, and R^p represents the P-wave radiation pattern (Aki and Richards, 2002). Since $\Delta\sigma$ slightly differs from the static stress drop, it may be more accurate to refer to it as the dynamic stress drop (Boatwright, 1980; Mori, 1983). The derivative of a step function results in a delta function, thus making it impossible to measure a slope as in equation (2). However, this is merely a mathematical singularity, which is lost through various physical processes, including the finite time for the stress drop on the fault plane, the internal attenuation and scattering that dampen seismic waves during propagation, and various heterogeneities at the source. In actual observations, the influence of site characteristics at the station is also significant.

As we will demonstrate, the distance dependency described by equation (4) is not consistent with the observed distance dependency of B. In the original $B-\Delta$ method, it is assumed that B values depend on the epicentral distance. However, considering that we are observing the properties of seismic waves that change with wave propagation, it is physically reasonable to consider these values as dependent on propagation distance or travel time. Therefore, this study examines the relationship between B and T_p. Since this relationship may not be approximated by a simple function, we first estimate a functional form that represents the dependency on T_p. As shown in Results, when fixing a certain range of T_p, the distribution of estimated B values approximately follow a log-normal distribution (Figure S3). However, some deviations from this approximation appear when the sample size is small. Therefore, we estimate the function $f(T_p)$ as the median of the distribution of $\log_{10} B$. We have confirmed that the results do not significantly change when analyzed using the mean instead.

The discrepancies between individual observed values of $\log_{10} B$ and the approximation function $f(T_p)$ include contributions from both the source process and wave propagation process. We hypothesize that for the i-th earthquake observed at the j-th station, the observed value of $\log_{10} B$ can be represented as:

$$\log_{10} B^{ij}_{obs} = f(T^{ij}_{p\,obs}) + c \log_{10} R^p + E_i + S_j + e_{ij} \quad (5)$$

where E_i relates to the source process, S_j to the wave propagation process, and c is a constant. Assuming error e_{ij} follows a normal distribution, maximum likelihood estimation can be applied to estimate these parameters. Compared to equation (4), the source term E_i includes the stress drop and the velocity of rupture propagation at the source. If the propagation velocity is assumed to be constant, as suggested by Mori (1983), E_i is considered a deviation from the logarithmic mean of the initial stress drop. On the other hand, S_j contains effects from the density and P-wave speed, from the source to the site, with the site characteristics assumed to be particularly significant. Hereafter, S_j will be referred to as the site term, which is the deviation from the logarithmic mean of site amplification factor. Naturally, c is 1 compared to equation (4), but empirically, it has been necessary to include it as an unknown parameter. The reasons and interpretations for this will be explained in the Results section.

Average Source Parameters for Each Event

One of the primary objectives of this study is to compare the initial rupture process with the overall rupture process. For many of the earthquakes investigated in this study, Yoshida and Kanamori (2023) estimated the apparent moment rate function (AMRF) using a deconvolution method that employs empirical Green's functions for SH waves. This method is independent of the analysis of P-wave onsets used in this study. We examine the correlation between the source term E_i and AMRF for 1145 earthquakes common to both event groups.

Yoshida and Kanamori (2023) estimated seismic wave energy and source duration T, as parameters representing the AMRF. From these parameters they also derived scaled energy, duration-normalized moment, and a parameter representing earthquake complexity, REEF (Ye et al., 2018). These quantities are almost scale-invariant, showing little dependence on seismic moment. The estimation of the seismic energy is significantly affected by corrections outside the analyzed frequency range. Therefore, we examine the duration estimated directly from the AMRF, rather than scaled energy and REEF, which include these corrections. They obtained an estimate of the median value of duration-normalized moment M_0/T^3 as 3.5×10^{16} Nm/s/s/s, which corresponds to a relationship between M_W and T as:

$$T(s) \sim 10^{(M_W - 4.96)/2} \tag{6}$$

Equation (6) gives T of approximately 1 s for M_W 5, which is consistent with previous seismological knowledge.

The duration T should be compared carefully with the time window length used in this study. For instance, at the lower analytical limit corresponding to M_W 3.1-3.3, T is 0.12-0.15 s from equation (6). In this case, even with the previously assumed time window length of 0.1 s is longer than a half of T, which necessitates caution in interpreting behaviors at the lower end of the distribution. Additionally, for a 0.4 s time window, equation (6) results in M_W 4.16, which might include biases corresponding to M_W below 4. To assume a part of the source as the initial phase, a time window about a quarter of T would be appropriate. Even with a 0.1 s time window, it becomes necessary to focus the discussion on earthquakes above M_W 4.

RESULTS

Estimated B Values and Travel Time Dependence

Figure 3a presents a log-log plot showing estimated values of B against T_p. The variability in B is substantial, nearly an order of magnitude. When plotted on a semi-log graph (Figure S4), the maximum values of B decrease almost linearly, or exponentially, with T_p. This trend may be explained by geometrical and intrinsic attenuations that are proportional to $e^{-(\pi f T_p)/Q}/T_P$, where $f/Q = 0.05 - 0.1$ (for example, $f = 10$ Hz and $Q = 100 - 200$). On the other hand, when creating histograms for every 0.04 range on the log10 scale, B approximately follows a log-normal distribution (Figure S3). Neither the mean nor the median of this distribution can be approximated by an exponential function of T_p. Instead, B decreases with a slope corresponding to the square to the fourth power of T_p (Figure 3b). A function representing the standard values of $\log_{10} B$ is derived from the median values of the bins. This function is $f(T_p)$.

As previously noted, this distribution does not depend on the size of the earthquake. This fact is confirmed by Figure S5a, which displays the estimates for $M_w < 4$ and $M_w > 5$ in different colors. These results are based on a 0.1 s time window; similar results displayed for 0.2-0.4 s windows show an upward bias in the estimates for larger earthquakes (Figure S5b-d). The implications of such biases will be discussed later.

Effect of P-wave Radiation Pattern

The values of B once the standard value $f(T_p)$ is subtracted reflect the influences of the P-wave radiation pattern, the source process, and the propagation process. We first investigate the dependency of B on the radiation pattern. Figure 4 displays the values of $B - f(T_p)$ plotted against the radiation pattern R^p. According to a simple homogenous medium model like the one described by the formula (4), a larger radiation pattern should result in a positive deviation in the estimated values of B, which would correspond to $\log_{10} R^p$, implying that $c = 1$ in equation (5). However, this distribution cannot be explained with $c = 1$. Rather, it is better explained with $c \sim 0.5$, meaning the relationship is more accurately modeled by a square root of R^p. Linear regression yields a slope of 0.500 ± 0.012 (maximum likelihood estimate and standard error, using similar notation hereafter).

There are several important considerations to note. In the data pre-processing, waveforms with low signal-to-noise ratios were excluded, meaning that inherently weaker signals with small R^p were removed. As a result, the bottom of distribution in Figure 4 may be truncated, which might make the slope appear slightly smaller when simply fitting the distribution. Therefore, by converting the relationship between R^p and B into a two-dimensional histogram and taking the mode for each R^p value using the Kernel Density Estimation method, a slight deviation below the linear fit occurs at smaller R^p values, resulting in a slope of 0.631. However, this still significantly deviates from 1. Figure 4 is based on the result with a time window of 0.1 s ($N = 10$), but the trend remains unchanged even with a time window of 0.4 s ($N = 40$). These observations have led to the inclusion of c as an unknown parameter in equation (5).

The acceleration records used for estimating B were derived by simply differentiating the velocity waveforms, which predominantly contain high-frequency signals ranging from several Hz to several tens of Hz. Previous studies have reported that at such high frequencies, the radiation pattern becomes more isotropic, deviating from the double-couple pattern (Takemura et al., 2009; Kobayashi et al., 2015; Trugman et al., 2021). Near nodal planes, the amplitudes of the observed seismic waves at high frequencies are less likely to approach zero. The observations in Figure 4 could potentially be explained by the fact that the amplitude does not diminish near the nodal planes due to the analysis of high-frequency waveforms, similar to previous studies. However, there is a significant difference between this observation and previous research. Prior studies explained that the radiation pattern was smeared largely due to the contribution of coda waves, either from scattering near the source or during propagation. In contrast, this study, focusing on the onset, does not consider the contribution of later coda waves. It might be due to homogenization caused by forward scattering, or possibly because the rupture process itself deviates from a simple planer slip, or a double couple source, on a scale smaller than the resolution of the seismic waves, making the nodal planes indiscernible. Even small earthquakes may have a clear non-double-couple focal mechanism as demonstrated by recent dense observations (Hayashida et al., 2020).

Decomposition into Site and Event terms

Using equation (5) and taking $B - f(T_p)$ as the data, we estimated the source term E_i site term S_j, and the coefficient c through linear inversion within the range of $\log_{10} T_p$ from 0.1 to 1.3 (1.26 s < T_p < 19.95 s). However, equation (5) alone lacks one condition necessary to constrain all parameters. Therefore, we assumed prior information that both the event term E_i and site term S_j follow a normal distribution with a mean of zero and a variance of α^2, and estimated α using the Akaike Bayesian Information Criterion (ABIC, Akaike, 1980; Yabuki and Matsu'ura, 1992). The appropriate value of α was found to be 1.49. The standard deviation of the data, $B - f\left(T_p\right)$, was reduced from 0.559 to 0.399 for e_{ij}, achieving a variance reduction of approximately 47%. The coefficient c for the P-wave radiation pattern discussed in the previous section was estimated at 0.467. The standard deviations of the source and site terms were 0.271 and 0.198, respectively. Considering these as linear parameters like stress drop and site amplification rate, the variability corresponds to roughly a factor of 2-3.

Figure 5a shows the spatial distribution of the source and site terms. The source term appears to have slightly larger values, ranging from blue to green, on the western side of Honshu, although the variability is also significant. This period includes relatively large inland earthquakes such as the 2004 Chuetsu earthquake (M_w), the 2008 Iwate-Miyagi earthquake (M_w), the 2011 Fukushima earthquake (M_w), and the 2016 Kumamoto earthquake (M_w), around which many aftershocks occurred. In Figure 5 markers were plotted in descending order of event terms, making it appear that many earthquakes with small event term occurred in these regions; however, this is merely an artifact. The respective medians are -0.015, -0.034, 0.051, and 0.034, suggesting some regional biases, but the variability within each region is significantly greater than the biases associated with those regions (Figure 6).

The site terms also tend to be somewhat larger on the western side of Honshu. Since the pattern is similar to that of the source terms, it is unlikely that the two distributions are causing a trade-off effect. Along the plate boundary that divides eastern and western Japan, stations with smaller site terms appear to be aligned. This region also has many earthquakes with smaller source terms. Additionally, smaller site terms are observed in the Kii Peninsula, Shikoku, and eastern Kyushu, broadly corresponding to the Median Tectonic Line in western Japan. The structure beneath the Japanese islands is heterogeneous, and it is likely that these heterogeneities are included in what has been categorized as site terms in this study. While structure tomography using these site terms could provide insights into the subsurface structure, the present study focuses primarily on the source and does not delve further into these aspects.

Size and Depth Dependence of Event Terms

As previously reported, the estimated values of B little depend on the final earthquake size. Therefore, the dependence on magnitude will also be minimal in the decomposed event term. Figure 7a compares event terms with M_w. The slope is 0.040±0.014, which may appear significant at first glance. However, if the regression is limited to $M_w > 4$ for safety, the slope becomes 0.022±0.031, indicating some size dependence, but it is not statistically significant. This result corresponds to a time window of 0.1 s. Conducting a similar analysis with a 0.4 s time window yields results as shown in Figure S6, where the event term significantly depends on the magnitude. A 0.4 s window covers a period equal to or greater than the duration for most earthquakes with $M_w < 4$, potentially revealing characteristics of the entire source rather than just the initial process. This demonstrates why a short time window is critical for such analyses.

The event term exhibits a significant positive correlation with the source depth, as shown in Figure 7b. This trend is particularly notable for earthquakes at depths shallower than 10 km. Below 10 km, the variation is less significant. Since the event term is related to the initial stress drop, this suggests a depth dependence of the initial stress drop in earthquakes, as it is well-known that the overall stress drop of earthquakes depends on depth (Hardebeck and Hauksson, 1997; Shearer et al., 2006; Abercrombie, 2021). However, it is important to note that the rigidity of rocks changes with depth. It has been suggested that the depth dependence of rigidity could be causing the depth dependence of stress changes (Vallée, 2013), and a similar interpretation may be possible for Figure 7b.

Parameters from Initial and Whole Source Processes

Figure 8a compares the event term estimated from the initial P-waves with the normalized duration, $T/M_0^{1/3}$, derived from the AMRF duration in Yoshida and Kanamori (2023). When all data are considered, as the event term increases, the normalized duration decreases. A simple interpretation suggests that the larger the initial stress drop, the more likely the earthquake finishes in a shorter duration. Although the variability is large, the negative slope is statistically significant. While the event term exhibits depth dependence, the same trend is apparent when grouped by depth (Figure 8b-d). We also examined this correlation grouped by the final magnitude of the earthquakes (Figure 8e-f). For magnitudes less than 3.5, the time window length used to estimate the event term is not significantly different from T. Despite the small number of events, a noticeable correlation is apparent (Figure 8e). Interestingly, this trend persists even as the final size of the earthquakes increases, suggesting that the characteristics at the onset of an earthquake, specifically the initial stress drop, are related to the duration it takes for the earthquake to conclude. This trend is also observable in the four regions of major earthquakes shown in Figures 5a and 6, though the statistical significance is unclear due to the small sample size (Figure S7).

The results indicate a correlation between the initial and overall processes of earthquakes. However, this does not necessarily imply a causal relationship between the two. Rather than the initial process determining the overall process, it is possible that both are governed by the same characteristics near the source. For example, the elastic properties of the subsurface rocks in the region or the maturity of the fault system where the earthquake occurred might control both the initial and the overall processes.

DISCUSSION

Accuracy of JMA Pick Information

In this study, the accurate determination of the onset time of P-waves is crucial for the reliability of the results. The pick information of the JMA serves as training data for recent automatic earthquake detection algorithms based on machine learning (Naoi et al., 2024), and represent the best data currently available. To assess the accuracy of this information, we examined how the acceleration records we used change around the detection values. As illustrated in Figures 2 and S1, most are clearly recognized as distinct onsets. Furthermore, as objective evidence, we present a two-dimensional histogram of the amplitudes from 0.2 seconds before to 0.2 seconds after the detection values, using 26,767 acceleration records (Figure S8). As previously mentioned, records where the standard deviation of pre-signal noise, σ_{noise}, exceeds 10^{-5} m/s/s have been excluded, and we have imposed the condition that $\sigma_{signal}/\sigma_{noise} \geq \sqrt{10}$. An abrupt change in the distribution is observed right at the 0-second sample. The distribution one sample before shows almost no change from the distribution over the previous 0.2 seconds, confirming that there are few instances where detections are delayed by 0.01 seconds. Moreover, by 0.06 seconds later, there are small number of samples within the demonstrated acceleration range, indicating significantly larger amplitudes. Thus, it can be stated that the time window length of 0.1 s contains a signal substantially larger than the noise level for more than half of its duration.

Distance Estimation from B values

In our analysis thus far, we first approximated B as a function of the propagation time T_p, and then distributed the residuals between the source and site terms. To use B estimation at each station for EEW, it is necessary to know T_p from B, or approximate T_p as a function of B, i.e., $T_p(B)$. Therefore, we conducted a similar analysis with the axes in Figure 3 swapped. The $T_p(B)$ estimated from all data points where $-4.25 < B < -0.25$ appear significantly different from $B(T_p) =$

$10^{f(T_p)}$ (Figure 9). Consequently, the estimated source and site terms are not the same, though they show a high correlation. The site and event terms estimated for $B(T_p)$ are approximately four times those estimated for $T_p(B)$ (Figure S9). While individual event and site values differ, the estimations for spatial distribution and aftershock groups generally show similar trends to those in Figures 5 and 6 (Figures S10 and S11).

When estimating B at a specific station then deriving $T_p(B)$, the standard deviation in the log10 domain is 0.169, which corresponds to a factor of 1.47 (Figure 10a). However, it is crucial to note that there is a tendency to overestimate T_p, especially when real T_p is small, as shown in the upper left distribution of Figure 10a. For the purposes of EEW, estimating the source further than its actual location can be hazardous. When corrections for the site term, source term, and radiation pattern are all applied (green dots), the standard deviation decreases to 0.110. However, in real-time operation, neither the source term nor the radiation pattern is known. Correcting for the site term alone (orange dots) reduces the standard deviation to 0.133, approximately a 1.36-fold decrease, which tends to mitigate significant overestimations of T_p (Figure 10b). Correcting for the site term alone has practical significance.

Universal Earthquake Onset

This study successfully isolated characteristics of the initial rupture process that are largely independent of the final size of earthquakes. If such signals do not depend on the earthquake's final size, the processes generating these signals can be considered necessary conditions for the initiation of seismic rupture. We often identify "subevents" within a finite duration of seismic waves, and in some cases, these subevents are considered as distinct earthquakes. Most recently, in the 2024 Noto Peninsula earthquake, an earthquake of magnitude M_W 7.5 was preceded by two foreshocks events 13 and 14 seconds before the main event, respectively (Yoshida et al., 2024). Are these three separate earthquakes, or are they subevents? If there is a common initial rupture process across all earthquakes, it could serve as a criterion to distinguish between separate earthquakes and subevents.

Such common initial rupture process can be conceptualized as hierarchical rupture growth from minute nucleus, representing a quasi-two-dimensional rupture propagation process that includes some randomness. In contrast, a more developed rupture typically expands along a quasi-one-dimensional rupture front, and does not necessarily generate signals like the P-wave onset observed in earthquakes. In practical observations of natural earthquakes, once a rupture has sufficiently progressed, the complex wave radiation processes around the rupture front are likely to obscure smaller signals, rendering them undetectable. However, numerical simulations or controlled experiments might allow for the detection of such signals, potentially facilitating discussions about how many initial ruptures are contained within a single earthquake event.

CONCLUSION

In this study, we focused on the onset of P-wave acceleration, revealing that their amplitude is largely independent of earthquake size. Although this relationship has been known qualitatively, we were able to quantitatively assess it using high-quality seismograms from Hi-net, along with available mechanism solutions of F-net and manual picking information of JMA. The parameter B does not depend on the final size of the earthquake but is related to the distance from the source and travel time of P-wave. In our analysis, B was modeled as a function of travel time of P-wave and further decomposed into components dependent on each source, the propagation path—especially site characteristics—and radiation patterns. B decreases with the square to the fourth power of travel time of P-wave, a relationship that cannot be explained by simple geometric decay or intrinsic attenuation alone, suggesting it reflects properties of forward scattering of seismic waves. Theoretically, the radiation pattern should depend linearly on B, but practically, the dependency is less than linear, closer to a 0.5 power. The onset of acceleration waveforms occurs at relatively high frequencies, making it challenging to discern radiation pattern dependencies observed at lower frequencies. Moreover, this observation does not involve seismic coda waves, which have traditionally been used to explain such observations. Instead, it suggests that the initial rupture process, growing from minute sizes, may include complex rupture processes that smear the radiation pattern.

The source term primarily represents the initial stress drop, with variability nearly spanning an order of magnitude, similar to the variability observed in estimates of the overall stress drop of earthquakes (e.g., Abercrombie, 2021). The deeper the source, the larger the source term, which mirrors the characteristics observed in overall stress drop estimates. While regional biases are observed in the aftershock distributions of major earthquakes, the variability within each region is significantly greater. The final size of the earthquakes does not depend on B, but the 0.1 s time window used in this study can introduce apparent dependencies for earthquakes around magnitude M_w 3. Using longer time windows produces even larger apparent dependencies. It is crucial not to misunderstand such dependencies for the deterministic nature of earthquakes. The source term correlates with the duration normalized by the final earthquake size. In easy words, a rupture that starts off more vigorously tends to end relatively quickly, whereas one that starts slowly tends to last longer. The judgment made at 0.1 s (at the size of about M_w 3) influencing beyond M_w 4.5 to the final size indicates a deterministic nature from the initial signals and provides limited predictability about the nature of earthquakes.

The spatial distribution of the site terms estimated in this study is also of interest. Since the estimated site terms include effects from the wave propagation paths, it will be feasible in the future to compute the ray paths for each station and source combination, and to assess the seismic wave scattering characteristics along these paths. The propagation volume for seismic waves within 0.1 seconds of their arrival is extremely limited, which suggests a high resolution. However, the features of the spatial distribution are likely to be significantly influenced by the near-surface geology. The anomalies observed in the site terms near plate boundaries and major tectonic lines may be attributed to the influence of such large-scale structures on seismic wave scattering around the stations. B was originally introduced for EEW purposes. However, empirically estimating T_p from B can lead to falsely locate nearby earthquakes as being further away. Correcting solely for the site term can mitigate this issue, providing practical importance.

The observational parameter B, characterizing the onset of earthquakes, has not attracted much attention in the 20 years since its proposal. However, as demonstrated in this paper, it has the potential to bring new developments to earthquake research for various applications. Moreover, understanding of its nature, which is said to originate from scattering, is still evolving, and further progress in research is anticipated.

DATA AND RESOURCES

All seismic data are available at by the NIED Hi-net data server (https://www.hinet.bosai.go.jp/). Focal mechanisms are from NIED F-net (https://www.fnet.bosai.go.jp/event/search.php). Hypocenter and arrival time information are from the Seismological Bulletin of Japan of JMA (https://www.data.jma.go.jp/svd/eqev/data/bulletin/index_e.html). The Supplementary Material contains 11 supplementary figures.

DECLARATION OF COMPETING INTERESTS

The authors acknowledge there are no conflicts of interest recorded.

ACKNOWLEDGEMENTS

Figures are prepared using Geophysical Mapping Tools (Wessel et al., 2019) and Matplotlib (Hunter, 2007). This research has been supported by JSPS Kakenhi (21H04505), MEXT Kakenhi (21H05200, 24H01017), Earthquake and Volcano Hazards Observation and Research.

REFERENCES

Abercrombie, R. E., 2021, Resolution and uncertainties in estimates of earthquake stress drop and energy release, Philosophical Transactions of the Royal Society A: Mathematical, Physical and Engineering Sciences, 379, no. 2196, 20200131, doi: 10.1098/rsta.2020.0131.

Akaike, H., 1980, Likelihood and the Bayes procedure, Trabajos de Estadistica Y de Investigacion Operativa, 31, no. 1, 143–166, doi: 10.1007/BF02888350.

Aki, K., and P. Richards, 2002, Quantitative seismology, University Science Books.

Bird, P., 2003, An updated digital model of plate boundaries, Geochemistry, Geophysics, Geosystems, 4, no. 3, doi: 10.1029/2001GC000252.

Boatwright, J., 1980, A spectral theory for circular seismic sources; simple estimates of source dimension, dynamic stress drop, and radiated seismic energy, Bulletin of the Seismological Society of America, 70, no. 1, 1–27, doi: 10.1785/BSSA0700010001.

Brown, S. R., and C. H. Scholz, 1985, Broad bandwidth study of the topography of natural rock surfaces, Journal of Geophysical Research: Solid Earth, 90, no. B14, 12575–12582, doi: 10.1029/JB090iB14p12575.

Candela, T., F. Renard, Y. Klinger, K. Mair, J. Schmittbuhl, and E. E. Brodsky, 2012, Roughness of fault surfaces over nine decades of length scales, Journal of Geophysical Research: Solid Earth, 117, no. B8, doi: 10.1029/2011JB009041.

Colombelli, S., A. Zollo, G. Festa, and M. Picozzi, 2014, Evidence for a difference in rupture initiation between small and large earthquakes, 1, Nat Commun, 5, no. 1, 3958, doi: 10.1038/ncomms4958.

Dieterich, J. H., 1992, Earthquake nucleation on faults with rate-and state-dependent strength, Tectonophysics, 211, no. 1, 115–134, doi: 10.1016/0040-1951(92)90055-B.

Ellsworth, W. L., and G. C. Beroza, 1995, Seismic Evidence for an Earthquake Nucleation Phase, Science, 268, no. 5212, 851–855, doi: 10.1126/science.268.5212.851.

Festa, G., A. Zollo, and M. Lancieri, 2008, Earthquake magnitude estimation from early radiated energy, Geophysical Research Letters, 35, no. 22, doi: 10.1029/2008GL035576.

Gabriel, A.-A., D. I. Garagash, K. H. Palgunadi, and P. M. Mai, 2024, Fault size–dependent fracture energy explains multiscale seismicity and cascading earthquakes, Science, 385, no. 6707, eadj9587, doi: 10.1126/science.adj9587.

Hardebeck, J. L., and E. Hauksson, 1997, Static stress drop in the 1994 Northridge, California, aftershock sequence, Bulletin of the Seismological Society of America, 87, no. 6, 1495–1501, doi: 10.1785/BSSA0870061495.

Hayashida, Y., S. Matsumoto, Y. Iio, S. Sakai, and A. Kato, 2020, Non-Double-Couple Microearthquakes in the Focal Area of the 2000 Western Tottori Earthquake (M 7.3) via Hyperdense Seismic Observations, Geophysical Research Letters, 47, no. 4, e2019GL084841, doi: 10.1029/2019GL084841.

Hoshiba, M., O. Kamigaichi, M. Saito, S. Tsukada, and N. Hamada, 2008, Earthquake Early Warning Starts Nationwide in Japan, Eos, Transactions American Geophysical Union, 89, no. 8, 73–74, doi: 10.1029/2008EO080001.

Hunter, J. D., 2007, Matplotlib: A 2D Graphics Environment, Computing in Science & Engineering, 9, no. 3, 90–95, doi: 10.1109/MCSE.2007.55.

Ide, S., 2019, Frequent observations of identical onsets of large and small earthquakes, Nature, 573, no. 7772, 112–116, doi: 10.1038/s41586-019-1508-5.

Ide, S., and H. Aochi, 2005, Earthquakes as multiscale dynamic ruptures with heterogeneous fracture surface energy, Journal of Geophysical Research: Solid Earth, 110, no. B11, doi: 10.1029/2004JB003591.

Iio, Y., 1995, Observations of the slow initial phase generated by microearthquakes: Implications for earthquake nucleation and propagation, Journal of Geophysical Research: Solid Earth, 100, no. B8, 15333–15349, doi: 10.1029/95JB01150.

Iwata, N., S. Yamamoto, M. Korenaga, and S. Noda, 2015, Improved Algorithms of Seismic Parameters Estimation and Noise Discrimination in Earthquake Early Warning, Quarterly Report of RTRI, 56, no. 4, 291–298, doi: 10.2219/rtriqr.56.4_291.

Kobayashi, M., S. Takemura, and K. Yoshimoto, 2015, Frequency and distance changes in the apparent P-wave radiation pattern: effects of seismic wave scattering in the crust inferred from dense seismic observations and numerical simulations, Geophysical Journal International, 202, no. 3, 1895–1907, doi: 10.1093/gji/ggv263.

Kostrov, B. V., 1964, Selfsimilar problems of propagation of shear cracks, Journal of Applied Mathematics and Mechanics, 28, no. 5, 1077–1087, doi: 10.1016/0021-8928(64)90010-3.

Meier, M.-A., T. Heaton, and J. Clinton, 2016, Evidence for universal earthquake rupture initiation behavior, Geophysical Research Letters, 43, no. 15, 7991–7996, doi: 10.1002/2016GL070081.

Mori, J., 1983, Dynamic stress drops of moderate earthquakes of the Eastern Aleutians and their relation to a great earthquake, Bulletin of the Seismological Society of America, 73, no. 4, 1077–1097, doi: 10.1785/BSSA0730041077.

Mori, J., and H. Kanamori, 1996, Initial rupture of earthquakes in the 1995 Ridgecrest, California Sequence, Geophysical Research Letters, 23, no. 18, 2437–2440, doi: 10.1029/96GL02491.

Naoi, M., K. Tamaribuchi, K. Shimojo, S. Katoh, and S. Ohyanagi, 2024, Neural phase picker trained on the Japan meteorological agency unified earthquake catalog, Earth, Planets and Space, 76, no. 1, 150, doi: 10.1186/s40623-024-02091-8.

Noda, S., and W. L. Ellsworth, 2016, Scaling relation between earthquake magnitude and the departure time from P wave similar growth, Geophysical Research Letters, 43, no. 17, 9053–9060, doi: 10.1002/2016GL070069.

Odaka, T., K. Ashiya, S. Tsukada, S. Sato, K. Ohtake, and D. Nozaka, 2003, A New Method of Quickly Estimating Epicentral Distance and Magnitude from a Single Seismic Record, Bulletin of the Seismological Society of America, 93, no. 1, 526–532, doi: 10.1785/0120020008.

Okamoto, K., and S. Tsuno, 2019, Accuracy improvement in the estimation of epicentral distance inferred from initial P-waves by considering local heterogeneity, Exploration Geophysics, 50, no. 2, 159–171, doi: 10.1080/08123985.2019.1577681.

Olson, E. L., and R. M. Allen, 2005, The deterministic nature of earthquake rupture, 7065, Nature, 438, no. 7065, 212–215, doi: 10.1038/nature04214.

Power, W. L., and T. E. Tullis, 1991, Euclidean and fractal models for the description of rock surface roughness, Journal of Geophysical Research: Solid Earth, 96, no. B1, 415–424, doi: 10.1029/90JB02107.

Renou, J., M. Vallée, and H. Aochi, 2022, Deciphering the Origins of Transient Seismic Moment Accelerations by Realistic Dynamic Rupture Simulations, Bulletin of the Seismological Society of America, doi: 10.1785/0120210221.

Rydelek, P., and S. Horiuchi, 2006, Is earthquake rupture deterministic?, 7100, Nature, 442, no. 7100, E5–E6, doi: 10.1038/nature04963.

Sato, T., and T. Hirasawa, 1973, Body Wave Spectra from Propagating Shear Cracks, Journal of Physics of the Earth, 21, no. 4, 415–431, doi: 10.4294/jpe1952.21.415.

Shearer, P. M., G. A. Prieto, and E. Hauksson, 2006, Comprehensive analysis of earthquake source spectra in southern California, Journal of Geophysical Research: Solid Earth, 111, no. B6, doi: 10.1029/2005JB003979.

Shibazaki, B., and M. Matsu'ura, 1992, Spontaneous processes for nucleation, dynamic propagation, and stop of earthquake rupture, Geophysical Research Letters, 19, no. 12, 1189–1192, doi: 10.1029/92GL01072.

Takemura, S., T. Furumura, and T. Saito, 2009, Distortion of the apparent S-wave radiation pattern in the high-frequency wavefield: Tottori-Ken Seibu, Japan, earthquake of 2000, Geophysical Journal International, 178, no. 2, 950–961, doi: 10.1111/j.1365-246X.2009.04210.x.

Trugman, D. T., S. X. Chu, and V. C. Tsai, 2021, Earthquake Source Complexity Controls the Frequency Dependence of Near-Source Radiation Patterns, Geophysical Research Letters, 48, no. 17, e2021GL095022, doi: 10.1029/2021GL095022.

Trugman, D. T., M. T. Page, S. E. Minson, and E. S. Cochran, 2019, Peak Ground Displacement Saturates Exactly When Expected: Implications for Earthquake Early Warning, Journal of Geophysical Research: Solid Earth, 124, no. 5, 4642–4653, doi: 10.1029/2018JB017093.

Tsukada, S., T. Odaka, K. Ashiya, K. Ohtake, and D. Nosaka, 2004, Analysis of the Envelope Waveform of the Initial Part of P-waves and its Application to Quickly Estimating the Epicentral Distance and Magnitude, Zishin 2, 56, no. 4, 351–361, doi: 10.4294/zisin1948.56.4_351.

Uchide, T., and S. Ide, 2010, Scaling of earthquake rupture growth in the Parkfield area: Self-similar growth and suppression by the finite seismogenic layer, Journal of Geophysical Research: Solid Earth, 115, no. B11, doi: 10.1029/2009JB007122.

Ueno, H., 2002, Improvement of hypocenter determination procedures in the Japan Meteorological Agency (in Japanese with English abstract), 123 p.

Umeda, Y., 1990, High-amplitude seismic waves radiated from the bright spot of an earthquake, Tectonophysics, 175, no. 1, 81–92, doi: 10.1016/0040-1951(90)90131-Q.

Vallée, M., 2013, Source time function properties indicate a strain drop independent of earthquake depth and magnitude, Nat Commun, 4, no. 1, 2606, doi: 10.1038/ncomms3606.

Wessel, P., J. F. Luis, L. Uieda, R. Scharroo, F. Wobbe, W. H. F. Smith, and D. Tian, 2019, The Generic Mapping Tools Version 6, Geochemistry, Geophysics, Geosystems, 20, no. 11, 5556–5564, doi: 10.1029/2019GC008515.

Wu, Y.-M., and L. Zhao, 2006, Magnitude estimation using the first three seconds P-wave amplitude in earthquake early warning, Geophysical Research Letters, 33, no. 16, doi: 10.1029/2006GL026871.

Yabuki, T., and M. Matsu'ura, 1992, Geodetic data inversion using a Bayesian information criterion for spatial distribution of fault slip, Geophysical Journal International, 109, no. 2, 363–375, doi: 10.1111/j.1365-246X.1992.tb00102.x.

Yamada, T., and S. Ide, 2008, Limitation of the Predominant-Period Estimator for Earthquake Early Warning and the Initial Rupture of Earthquakes, Bulletin of the Seismological Society of America, 98, no. 6, 2739–2745, doi: 10.1785/0120080144.

Ye, L., H. Kanamori, and T. Lay, 2018, Global variations of large megathrust earthquake rupture characteristics, Science Advances, 4, no. 3, eaao4915, doi: 10.1126/sciadv.aao4915.

Yoshida, K., and H. Kanamori, 2023, Time-domain source parameter estimation of Mw 3–7 earthquakes in Japan from a large database of moment-rate functions, Geophysical Journal International, 234, no. 1, 243–262, doi: 10.1093/gji/ggad068.

Yoshida, K., R. Takagi, Y. Fukushima, R. Ando, Y. Ohta, and Y. Hiramatsu, 2024, Role of a Hidden Fault in the Early Process of the 2024 Mw7.5 Noto Peninsula Earthquake, Geophysical Research Letters, 51, no. 16, e2024GL110993, doi: 10.1029/2024GL110993.

Postal Mailing Address

Satoshi Ide, Department of Earth and Planetary Science, Graduate School of Science, The University of Tokyo, 7-3-1 Hongo, Bunkyo, Tokyo, 113-0033, Japan

Keisuke Yoshida, Research Center for Prediction of Earthquakes and Volcanic Eruptions, Graduate School of Science, Tohoku University, 6-6 Aza-Aoba, Aramaki, Aoba-ku, Sendai, 980-8578, Japan

FIGURES

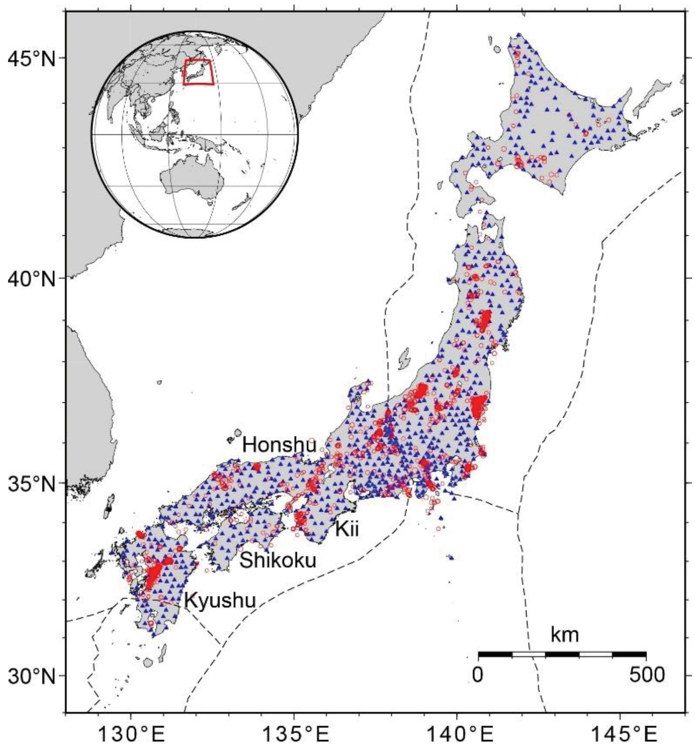

Figure 1. Distribution of earthquakes and Hi-net stations in the study area. Red circles and blue triangles represent earthquakes and stations, respectively. Dashed lines represent plate boundaries (Bird, 2003). The study area is indicated on the inset globe.

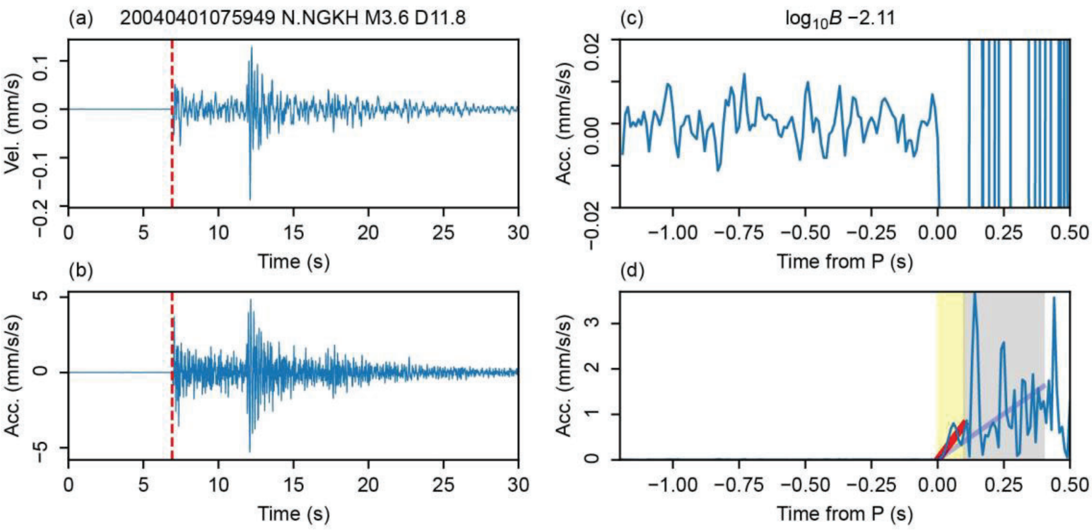

Figure 2. Example of estimating B. (a) Raw velocity seismogram. The dashed red line

indicates the arrival time of the P-wave. (b) Acceleration seismogram. (c) Close-up of (b) around the P-wave onset. (d) Absolute acceleration. Yellow and gray rectangles show the 0.1 and 0.4 s time windows from the P-wave onset, respectively. Red and purple lines represent B calculated in 0.1 and 0.4 s time windows, respectively.

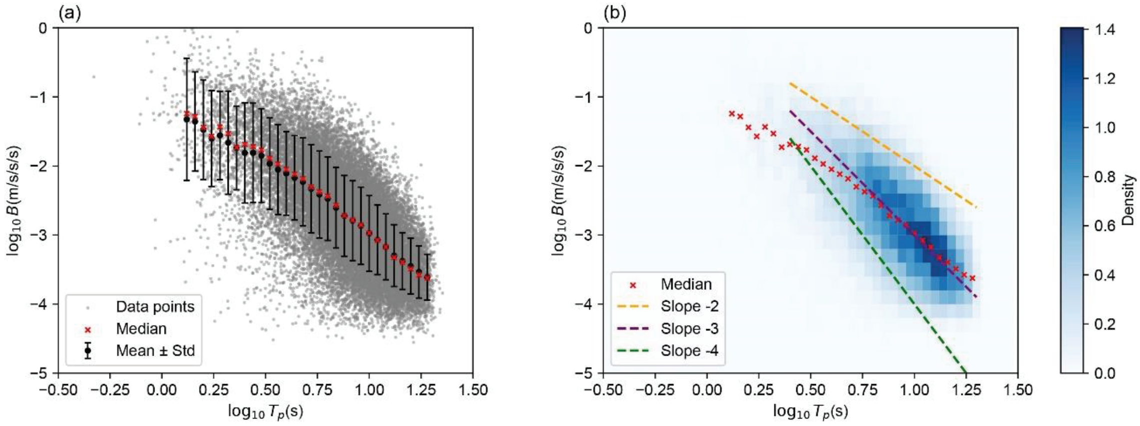

Figure 3. Estimated B value and P-wave travel time. (a) Scatter plot with gray dots representing all data points. Red crosses indicate the median $\log_{10} B$ in each bin with a width of 0.04. Black circles with error bars show the mean and standard error. (b) Two-dimensional histogram with orange, purple, and green lines representing slopes of −2, −3, and −4, respectively. Red crosses indicate the median.

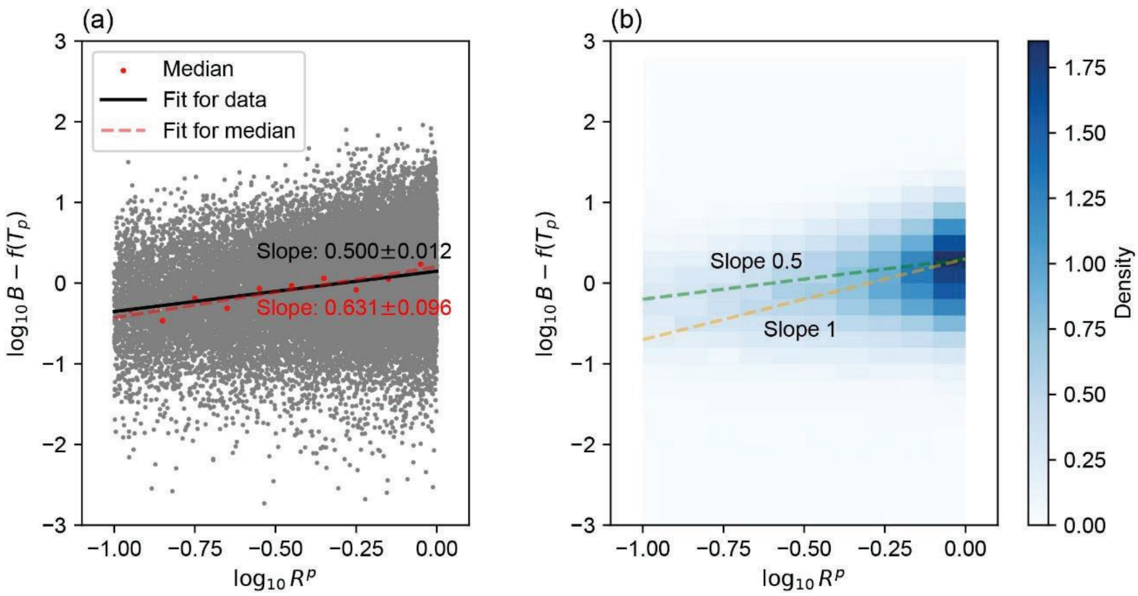

Figure 4. P-wave radiation pattern and B. (a) Each gray dot represents the value of $B -$

$f(T_p)$ for an event with a given radiation pattern R_p at a station. A black line shows a linear fit to these dots. Red dots represent the medians of gray dots measured in each 0.04 interval of $\log_{10} R_p$. A red line shows a linear fit to these median values. (b) Two-dimensional histogram with orange and green lines representing slopes of 1 and 0.5, respectively.

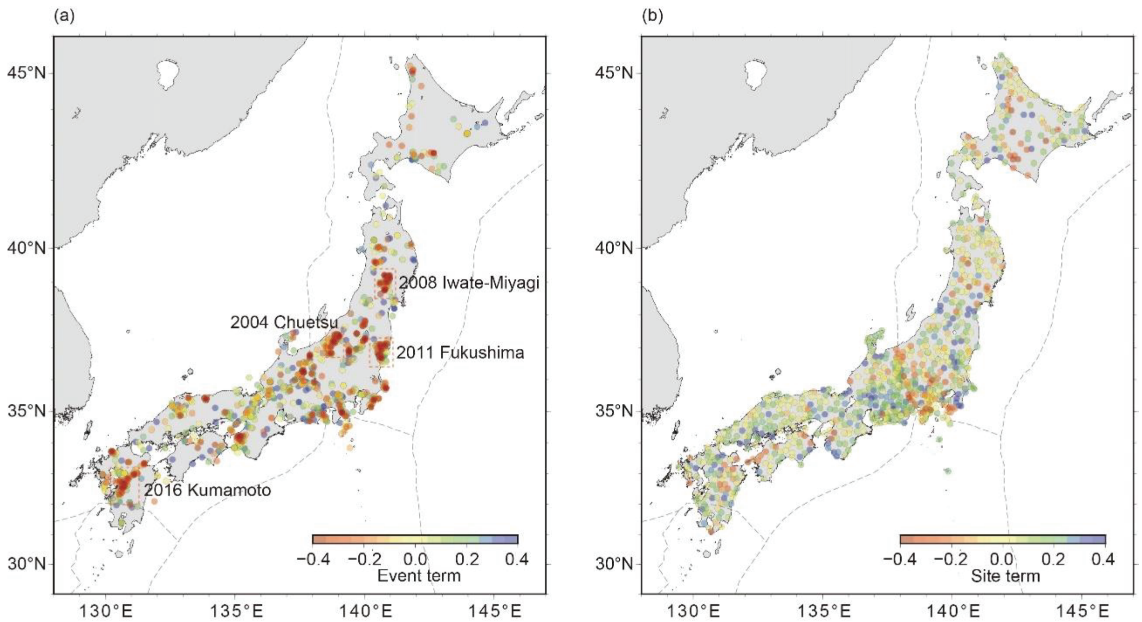

Figure 5. Spatial distribution of event and site terms. (a) Color-coded circles represent event terms. Red rectangles indicate the aftershock areas of four major earthquakes as shown. Dashed lines represent plate boundaries (Bird, 2003). (b) Color-coded circles represent site terms.

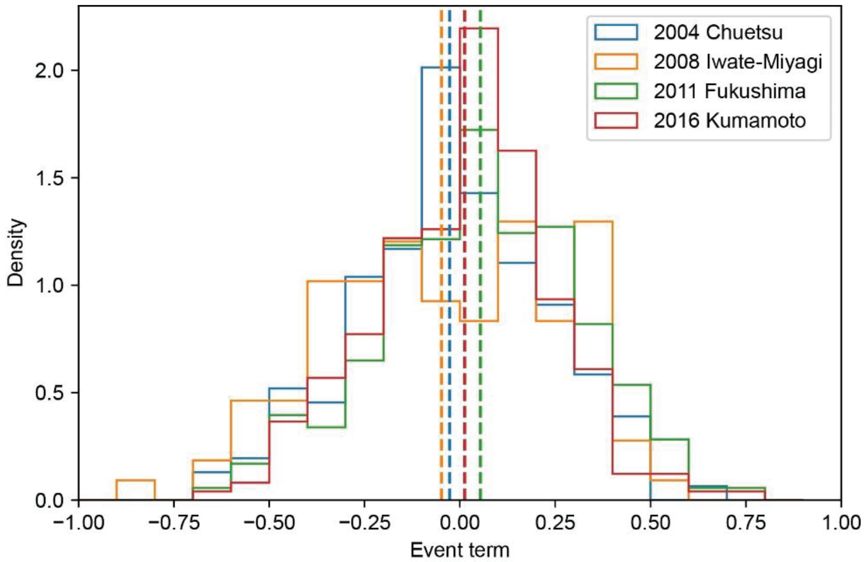

Figure 6. Event term distribution for aftershocks of four major earthquakes. Each event is shown in a different color as a density plot histogram, with a dashed line representing the median value.

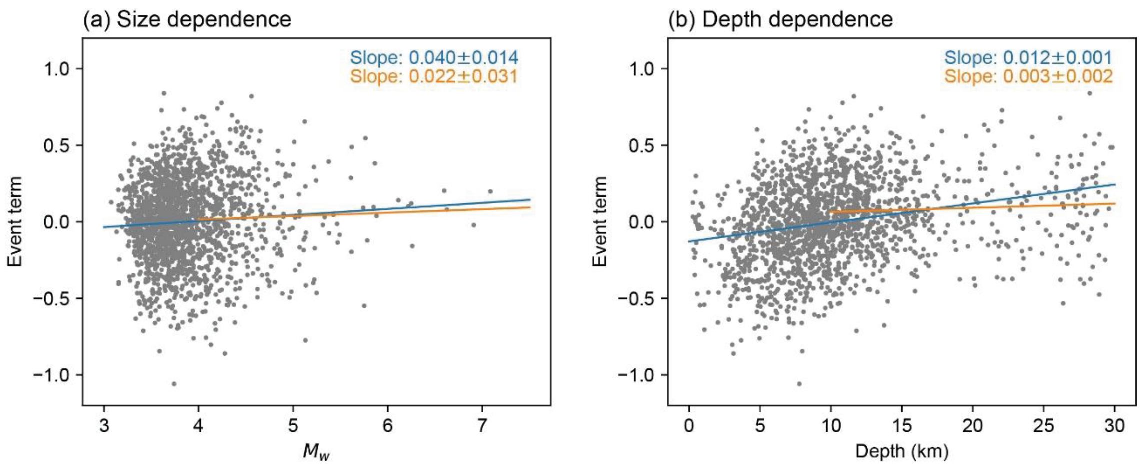

Figure 7. Size and depth dependence of event terms. (a) Magnitude dependence: Blue and orange lines represent the linear fits for all events and events larger than M_w 4, respectively. (b) Depth dependence: Blue and orange lines represent the linear fits for all events and events deeper than 10 km, respectively.

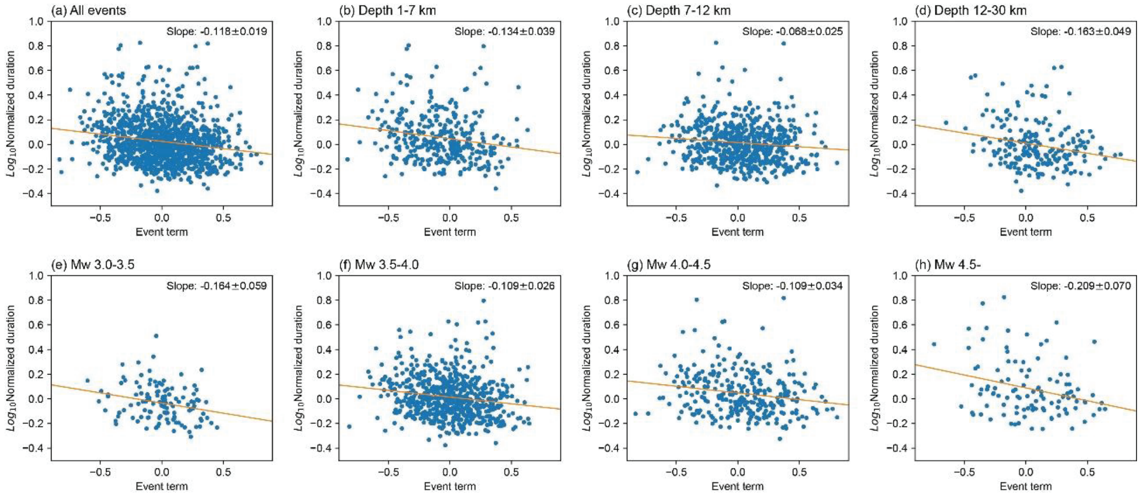

Figure 8. Comparison between event terms and normalized duration. (a) For all events, with an orange line showing a linear fit to the samples. (b)-(d) For events at different depths: 1-7 km, 7-12 km, and 12-30 km, respectively. (e)-(h) For events within different magnitude ranges, $3.0 < M_w < 3.5$, $3.5 < M_w < 4.0$, $4.0 < M_w < 4.5$, $4.5 < M_w$, respectively.

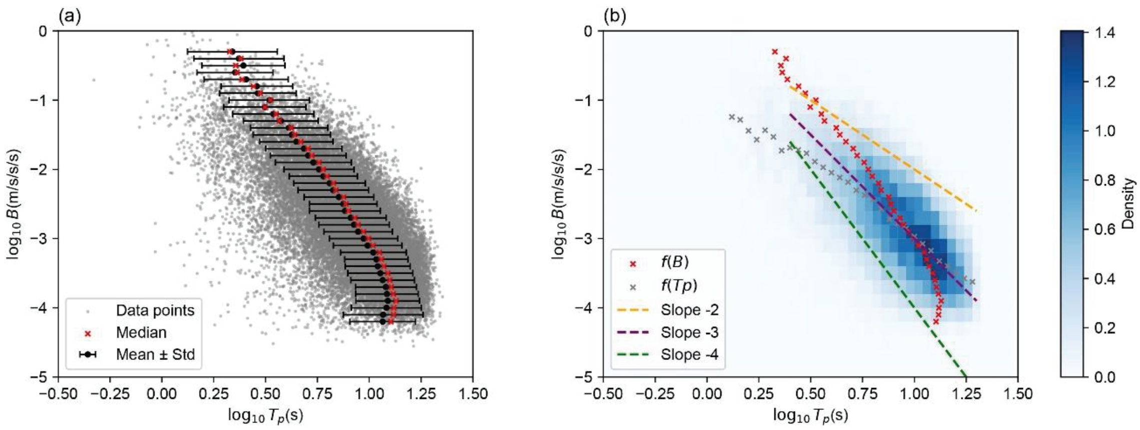

Figure 9. Estimated B value and P-wave travel time. (a) Scatter plot with gray dots representing all data points. Red crosses indicate the median of $\log_{10} T_p$ in each bin with a width of 0.01. Black circles with error bars show the mean and standard error. (b) Two-dimensional histogram with orange, purple, and green lines representing slopes of −2, −3, and −4, respectively. Red and gray crosses indicate the median of $\log_{10} T_p$ and $\log_{10} B$.

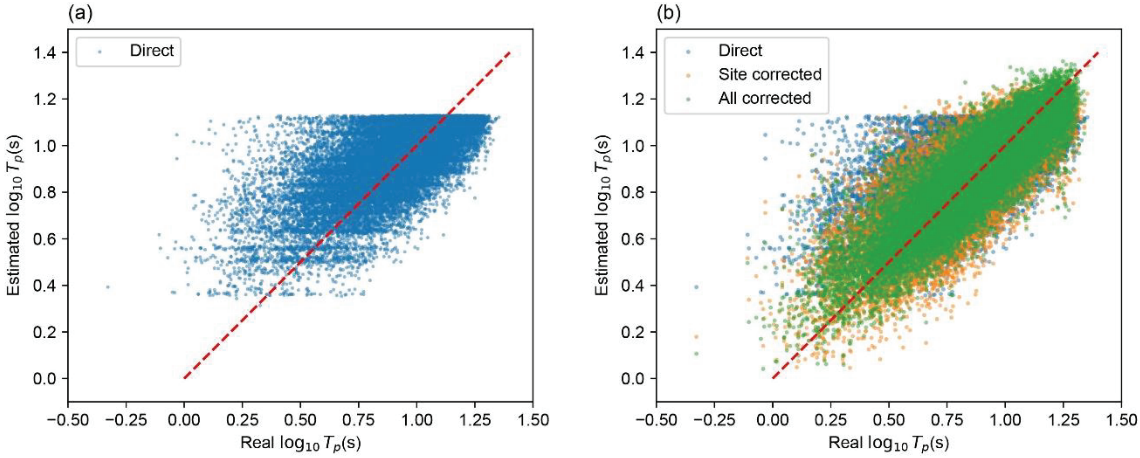

Figure 10. Predictability of T_p for EEW. (a) Comparison of actual arrival time and predictions using $f(B)$. (b) Blue dots are the same as in (a). Orange and green dots show comparisons of actual arrival time and prediction using $f(B)$ after correction of the site terms alone and all factors, respectively.

SUPPLEMENTAL MATERIAL: Predictable and Unpredictable Aspects of Earthquakes from P-wave Onsets: Vigorous Ruptures Finish Quickly

Satoshi Ide and Keisuke Yoshida

SUPPLEMENTARY FIGURES

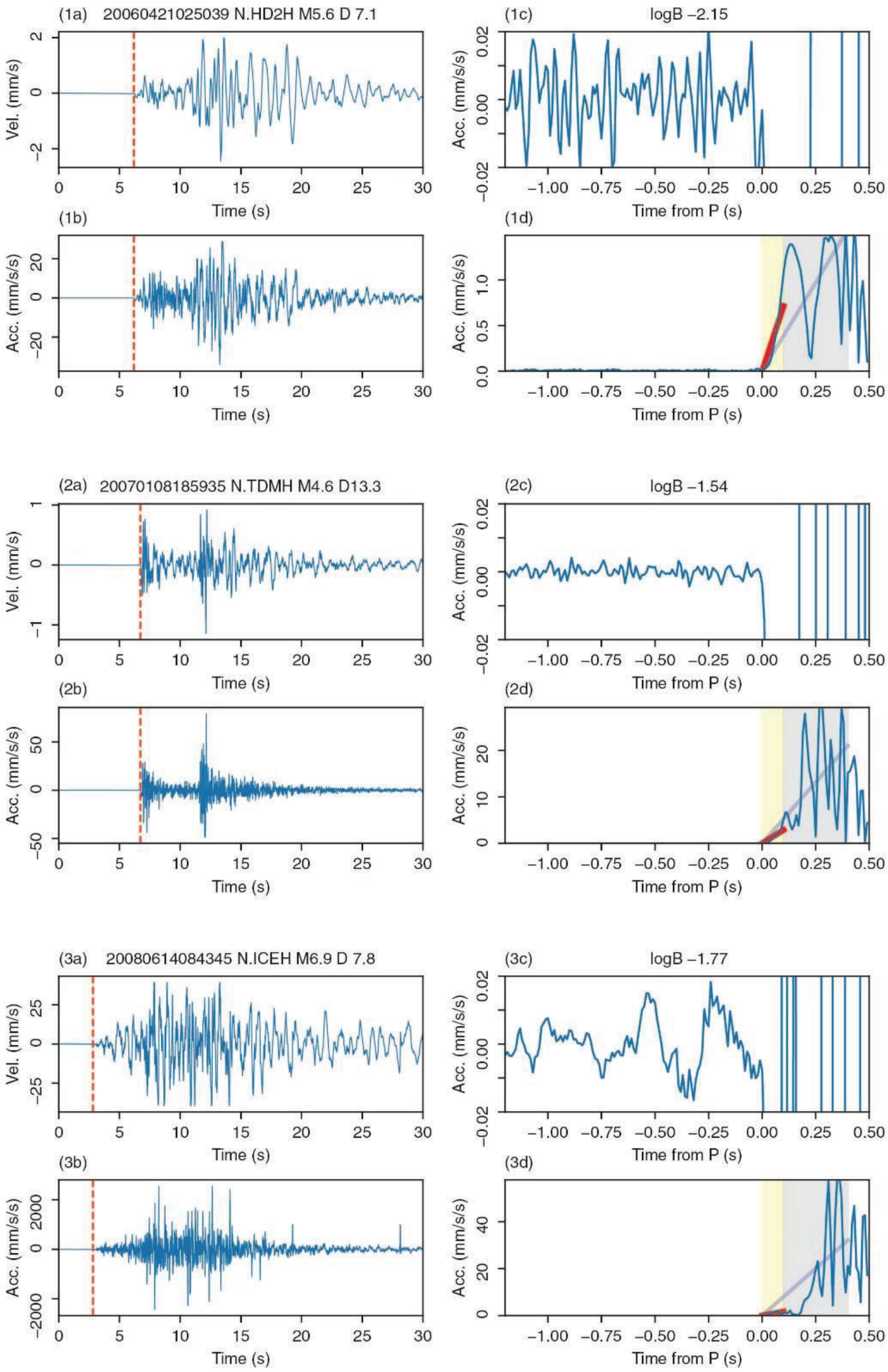

Figure S1. Example of estimating B for three events. (1a-3a) Raw velocity seismogram. The dashed red line indicates the arrival time of the P-wave. (1b-3b) Acceleration seismogram. (1c-3c) Close-up of (1b-3b) around the P-wave onset. (1d-3d) Absolute acceleration. Yellow and gray rectangles show the 0.1 and 0.4 s time windows from the P-wave onset, respectively. Red and purple lines represent B calculated in 0.1 and 0.4 s time windows, respectively.

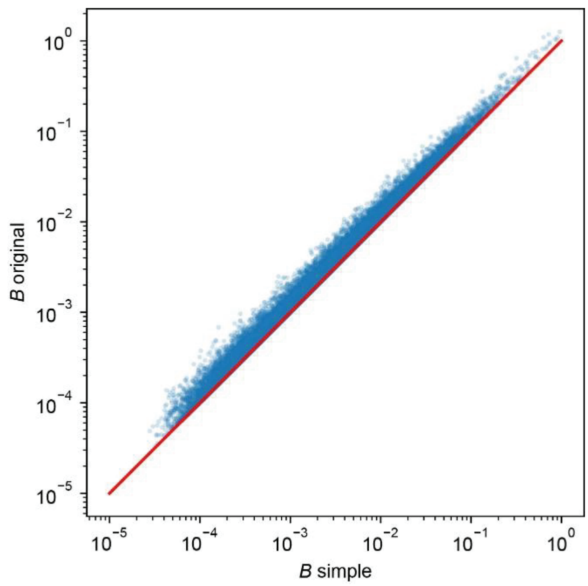

Figure S2. Comparison of B values estimated using the two slightly different definitions. The “simple” definition is utilized in the present study.

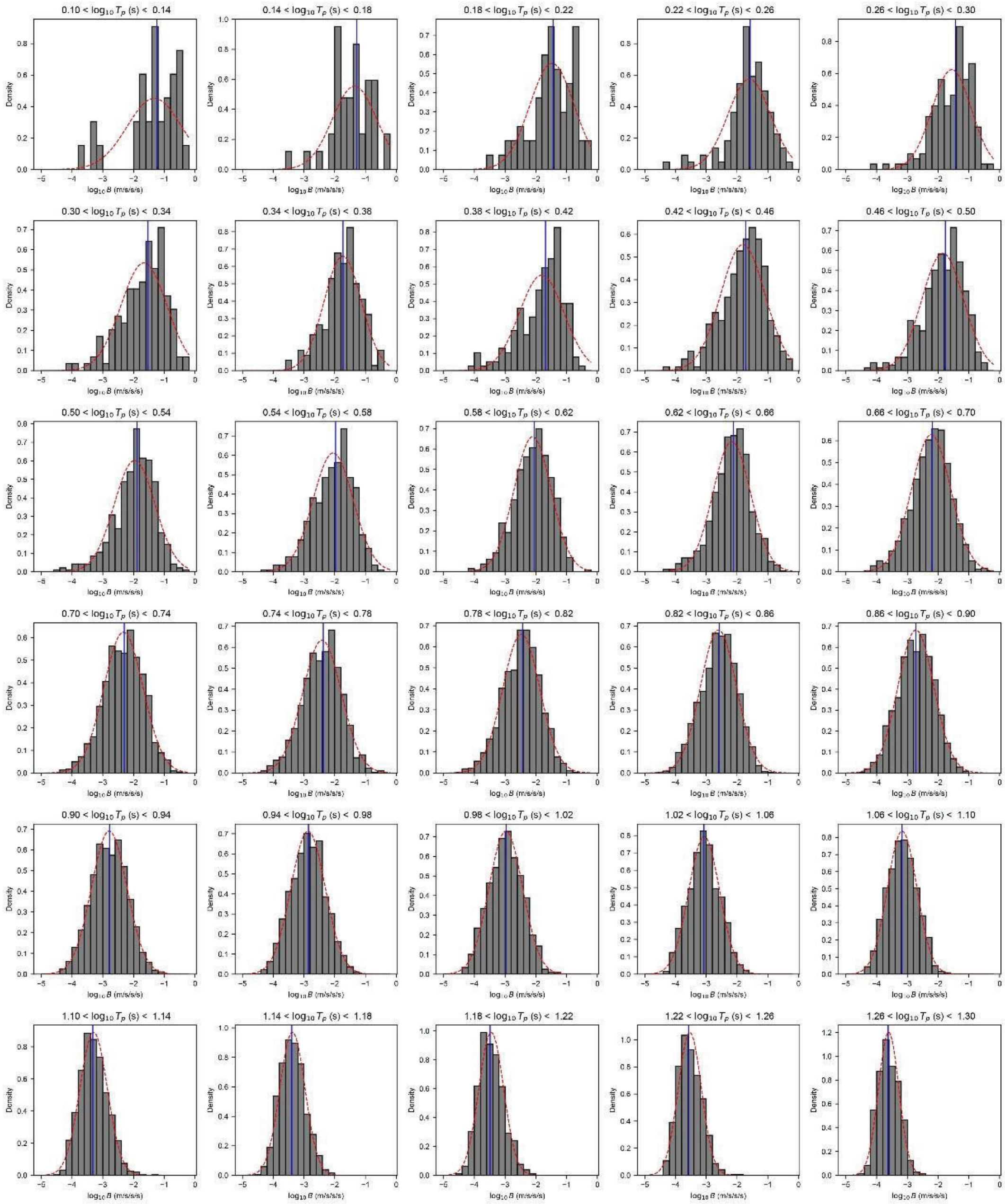

Figure S3. Histograms of estimated B values across different P-wave travel times (T_p). Each panel shows a density histogram of $\log_{10} B$ within a range of $\log_{10} T_p$, with a dashed red curve representing the corresponding normal distribution and a vertical blue line representing the median.

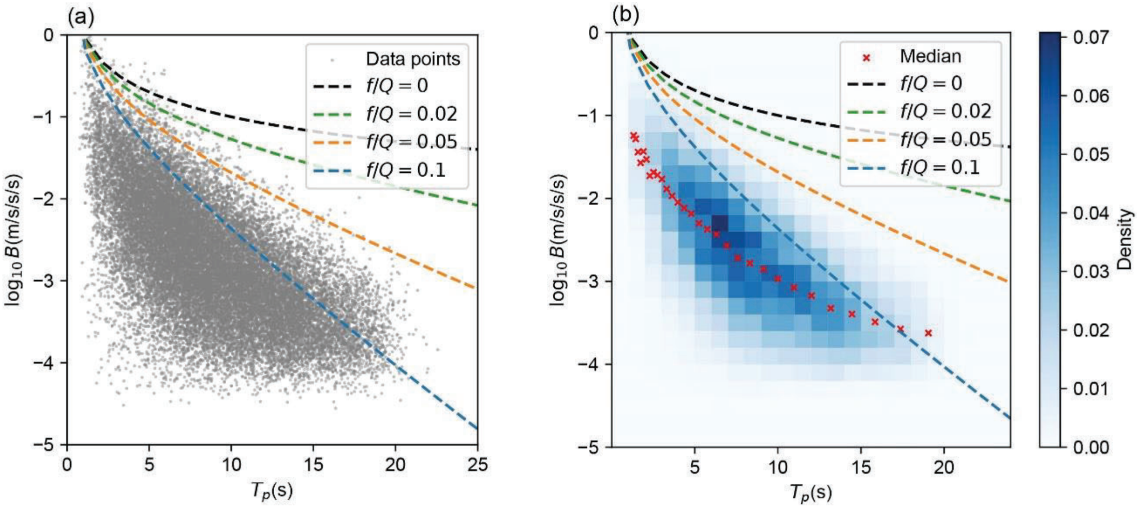

Figure S4. Estimated B value and P-wave travel time in a semi-log plot. (a) Scatter plot with gray dots representing all data points. Dashed lines indicate the attenuation curves with a constant f/Q of 0.0, 0.02, 0.05, and 0.1. (b) Two-dimensional histogram with the red dots shown in Figure 3.

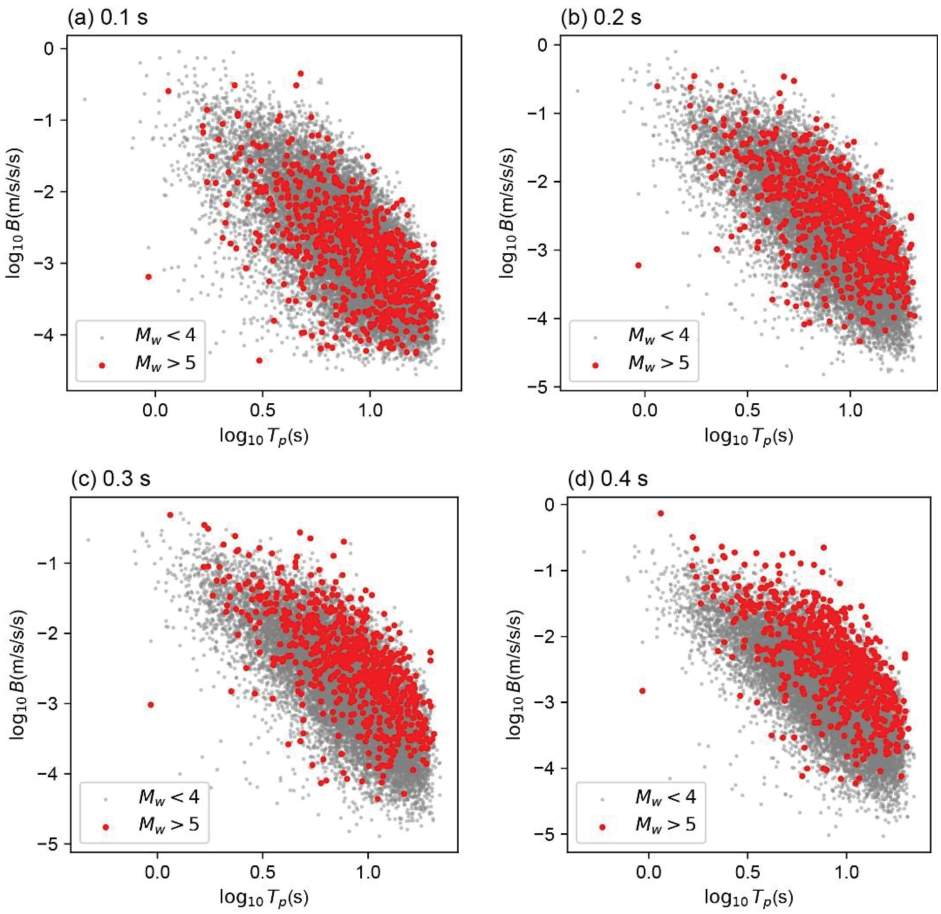

Figure S5. Estimated B value and P-wave travel time for different time windows. (a) For 0.1 s, with gray and red dots represent values for $M_w < 4$ and $M_w > 5$, respectively. (b) For 0.2 s. (c) For 0.3 s. (d) For 0.4 s.

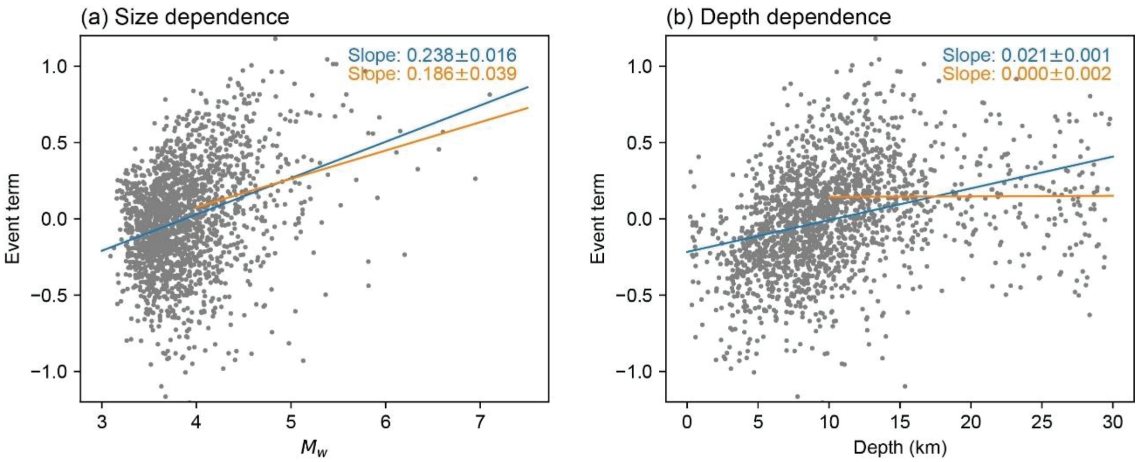

Figure S6. Size and depth dependence of event terms for a 0.4 s time window. (a) Magnitude dependence: Blue and orange lines represent the linear fits for all events and events larger than M_w 4, respectively. (b) Depth dependence: Blue and orange lines represent the linear fits for all events and events deeper than 10 km, respectively.

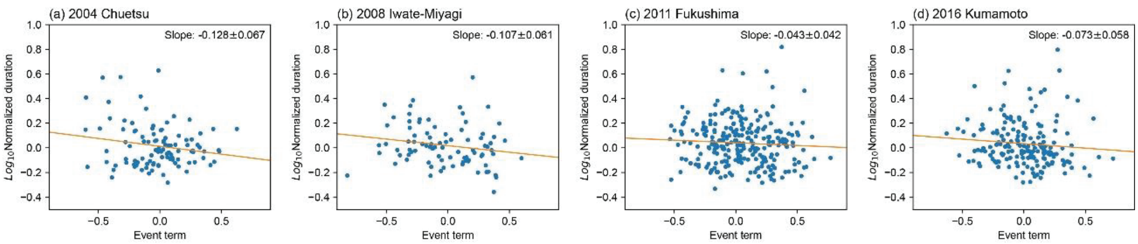

Figure S7. Comparison between event terms and normalized duration for the aftershock areas of four major earthquakes, with an orange line representing a linear fit to the samples.

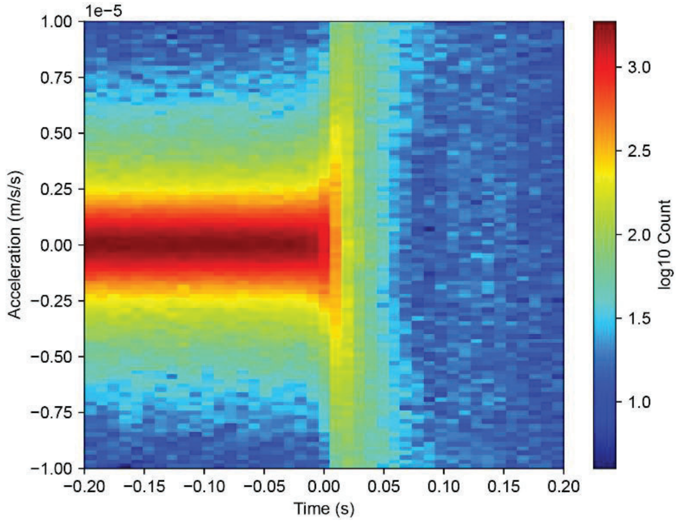

Figure S8. Accuracy of JMA arrival time information. This two-dimensional histogram shows the number of samples with specific accelerations and times relative to the P-wave arrival time.

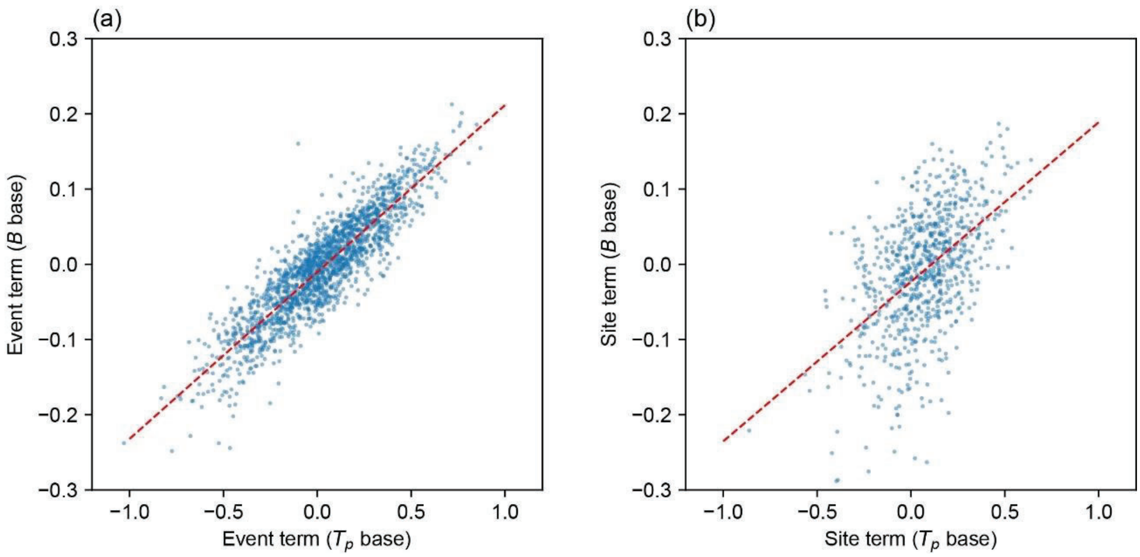

Figure S9. Comparison of event and site terms estimated from T_p and B. (a) Event terms. The dashed red line represents a linear fit with a slope of 0.222. (b) Site terms. The dashed red line represents a linear fit with a slope of 0.212.

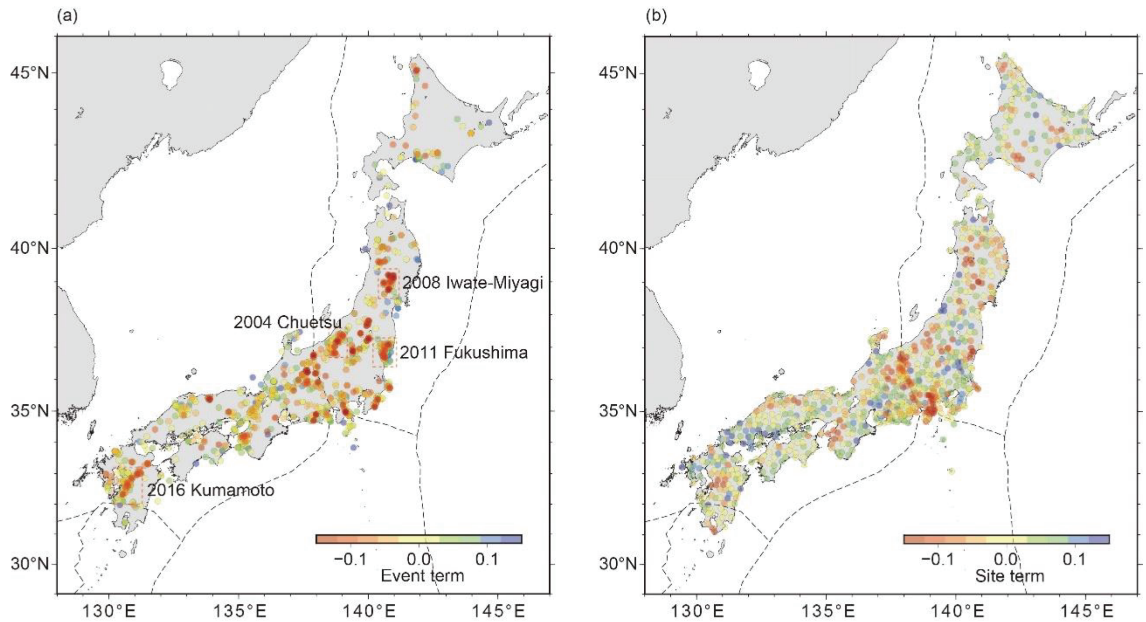

Figure S10. Spatial distribution of event and site terms, calculated from the residual of $T_p - f(B)$. (a) Color-coded circles represent event terms. Red rectangles indicate the aftershock areas of four major earthquakes as shown. Dashed lines represent plate boundaries (Bird, 2003). (b) Color-coded circles represent site terms.

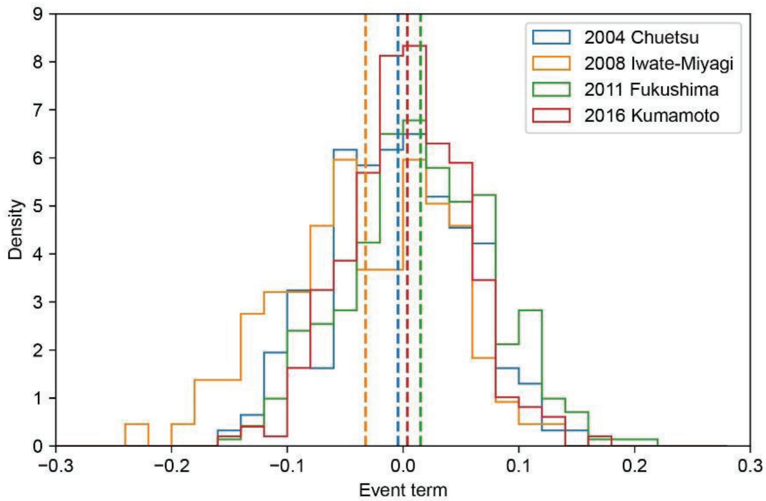

Figure S11. Event term distribution for aftershocks of four major earthquakes, calculated from the residual of $T_p - f(B)$. Each event is shown in a different color as a density plot histogram, with a dashed line representing the median value.